

Shock unsteadiness in a thrust optimized parabolic nozzle

S. B. Verma

Received: 7 May 2008 / Revised: 14 July 2008 / Accepted: 6 November 2008 / Published online: 29 November 2008
© Springer-Verlag 2008

Abstract This paper discusses the nature of shock unsteadiness, in an overexpanded thrust optimized parabolic nozzle, prevalent in various flow separation modes experienced during start up ($\delta P_0/\delta t > 0$) and shut down ($\delta P_0/\delta t < 0$) sequences. The results are based on simultaneously acquired data from real-time wall pressure measurements using Kulite pressure transducers, high-speed schlieren (2 kHz) of the exhaust flow-field and from strain-gauges installed on the nozzle bending tube. Shock unsteadiness in the separation region is seen to increase significantly just before the onset of each flow transition, even during steady nozzle operation. The intensity of this measure (*rms* level) is seen to be strongly influenced by relative locations of normal and overexpansion shock, the decrease in radial size of re-circulation zone in the back-flow region, and finally, the local nozzle wall contour. During restricted shock separation, the pressure fluctuations in separation region exhibit periodic characteristics rather than the usually observed characteristics of intermittent separation. The possible physical mechanisms responsible for the generation of flow unsteadiness in various separation modes are discussed. The results are from an experimental study conducted in P6.2 cold-gas subscale test facility using a thrust optimized parabolic nozzle of area-ratio 30.

Keywords Shock unsteadiness · Free shock separation · Restricted shock separation · Partially restricted shock separation · Side-loads

PACS 47.60.Kz

Communicated by A. Hadjadj.

S. B. Verma (✉)
Experimental Aerodynamics Division,
National Aerospace Laboratories (NAL), Bangalore 560017, India
e-mail: sbverma@ead.cmmacs.ernet.in

List of symbols

$G(f)$	power spectral density
f	sampling frequency, Hz
P_0	stagnation chamber pressure, bar
P_a	ambient pressure, bar
P_w	local mean wall pressure, bar
P_{pl}	plateau pressure after separation, bar
r_t	radius of nozzle throat, mm
X	co-ordinate along nozzle axis, mm
X_{sep}	point of physical separation, mm
X_{inc}	point of incipient separation, mm
X_{exit}	X-location of nozzle exit, mm
ϵ	area ratio of the nozzle
σ_{pw}	<i>rms</i> of the local wall pressure
$(\sigma_w/P_w)_{max}$	non-dimensionalized maximum value of <i>rms</i> pressure fluctuation
θ_{w_exit}	nozzle exit wall angle
θ_w	nozzle wall angle

Abbreviations

C_O	Overexpansion shock
C_R	Reflected shock
FSS	Free shock separation
NPR	Nozzle pressure ratio, P_0/P_a
pRSS	Partially restricted shock separation
qRSS	Quasi-restricted shock separation
RSS	Restricted shock separation
T	Triple point
TOP	Thrust optimized parabolic

1 Introduction

Most of the main stage rocket engine nozzles of modern day space launch vehicles such as the space shuttle main

engine (SSME) and Vulcain I & II use Rao's thrust optimized parabolic (TOP) contour design [1] primarily because of its high thrust/mass ratio. The need for such high vacuum performance engines requires high expansion rate in the divergent section of their nozzles. As a result during sea-level ignition (start up or shut down) or during low-altitude operation, these engines are necessarily overexpanded resulting in flow separation. Different separation modes have been detected and identified in the past [2,3] and the flow transition between these have been related to the observed side-load phenomena [4–7]. These are, namely free shock separation (FSS) wherein the flow does not reattach downstream of separation, Fig. 1a, and restricted shock separation (RSS) which experiences flow reattachment on nozzle wall downstream of separation resulting in the formation of a separation bubble, Fig. 1b. Numerical simulation studies of these modes [5] revealed the key driver to such flow transitions to be the momentum imbalance of flow passing through the overexpansion (C_O) and reflected shock (C_R), which is initiated by irregular/non-uniform rates of normal shock location movement relative to the separation shock location at different nozzle pressure ratio (NPR). More recently, it has also been found that the flow unsteadiness (in the separation region) preceding each flow transition between the separation modes to be related to the origin of side-loads in sub-scale nozzles [8].

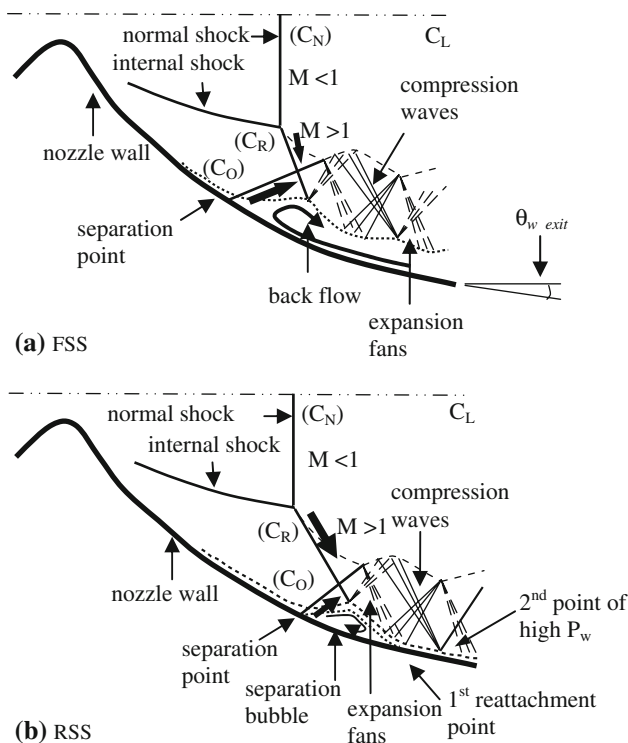


Fig. 1 Schematic of (a) free shock separation (FSS) and (b) restricted shock separation (RSS) condition inside a thrust optimized parabolic (TOP) nozzle

Side-loads have been observed both in sub-scale and full-scale rocket engine nozzles during their transient start up/shut down operation and also during steady engine operation with flow separation inside the nozzle [5]. This means the appearance of strong side-loads during the early phase of launcher's ascent can cause failure of the nozzle shell/engine and hence jeopardize the launch mission. Designing a robust nozzle to resist these loads would decrease the payload capacity of the launcher and hence reduce overall mission performance. Therefore, research to understand the existing flow transition phenomenology and the associated side-loads has emerged as an important area due to its impact on the design and performance of such nozzles. The seriousness of this issue is reflected by the recent sub-scale nozzle test campaigns performed in Europe [9–14] and Japan [15,16] both experimentally and numerically. A thorough understanding of the existing random and unsteady flow separation is therefore of importance in improving the nozzle performance.

Shock-wave boundary-layer interaction (SWBLI) flows are known to be inherently unsteady when the incoming boundary-layer is turbulent. Earlier studies on compression corners have revealed that the turbulent mixing gets considerably enhanced across the shock and this trend gets more pronounced with increase in shock strength [17]. Increase in shock strength also results in the separation shock to fan out more near its foot (due to thickening of the boundary layer caused by adverse pressure gradient) resulting in a system of compression waves that begin well ahead of the main fluctuating shock [18]. Dolling and Murphy [19] showed that because of this unsteady motion, the mean wall pressure begins to rise well ahead of the average shock position and this distance is found to increase with increase in shock strength. Kistler [20] and Dolling and Narlo [21] observed that the moving shock generates an intermittent signal whose level fluctuates between the range of characteristics of undisturbed boundary layer and that of disturbed flow downstream of shock (bi-modal signal). The spatial extent of these low-frequency large-amplitude wall pressure fluctuations is a strong function of shock strength [19,22,23]. In addition to the streamwise back-and-forth motion, the shock front was found by Muck et al. [23], Poggie et al. [24] and recently, by Verma and Haidn [25] to be wrinkled/split in the spanwise direction suggesting three-dimensionality of shock front.

The causes of flow unsteadiness are, however not completely understood. Based on observations and reasoning, several theories have been developed to understand the dynamics of separation shock as well as the physical mechanisms driving its motion. Smits and Dussauge [26] suggest the flow over the separated zone being sensitive to compression effects imposes unsteady conditions on the shock and makes it to move. A more convincing explanation was suggested by Maull [27] that the flow unsteadiness is caused by mass imbalance of fluid reversed at the reattachment point to

that scavenged from the separation point and is responsible for the ‘breathing’ motion of separation bubble. Charwat et al. [28] further reports that the model of mass-exchange appeared to yield more accurate semi-empirical correlations of measurements in separated flows. They therefore hypothesized that the separation bubble ‘breathes’ and during one-half of pulse, mass is injected into it while during the other half it is ejected out resulting into an unsteady mass-exchange. Such fluctuating pressure loads/unsteadiness of the shock-wave can have important implications on local heat transfer rates, noise generation and structural loading. The local peaks of heat transfer in the interaction region can be extremely severe and therefore pose a threat to the structural integrity of flight vehicles. A careful study and a thorough understanding of underlying phenomenon is therefore of practical and fundamental value at the design stage.

Studies discussing the unsteadiness linked to various flow separation modes in nozzle flows is very limited [29–32]. The goal of the current study is therefore to assess the nature of unsteady pressure fluctuations in the complete interaction region for different modes of separation to better understand the mechanisms in their generation. Different flow conditions prevalent during both start up and shut down are discussed. The test model used is the same TOP nozzle previously studied by Frey et al. [4] and Frey and Hagemann [5,6]. Stream-wise wall pressure measurement data are acquired along the nozzle contour using Kulites along with schlieren and surface oil-pigment visualization.

2 Experimental setup and procedure

2.1 Test facility

Tests were carried out in the cold flow test facility at P6.2 in DLR Lampoldshausen, Germany, on a horizontal test bench (Fig. 2a) and not in the closed altitude test chamber which limits visibility during test campaigns with surface oil flow, infrared thermometry etc. Gaseous nitrogen at ambient temperature is used as the test gas due to its advantage over compressed air, i.e., the absence of humidity and other impurities that can otherwise cause condensation of flow during operation. Under present test limitations, with the nozzle blowing into atmospheric pressure maximum pressure ratio up to 60 can be achieved.

The throat diameter of the sub-scale thrust optimized parabolic (TOP) nozzle used for the experimental investigation was 20 mm, yielding maximum mass flows in the range of $m = 4.2$ kg/s. A TOP nozzle of moderate area ratio (30) is used. Kulite type of pressure transducers (model XT-154–190M) have been used for wall pressure measurement both upstream and downstream of the throat. Four such pressure sensors are placed in the stagnation chamber and 13 along

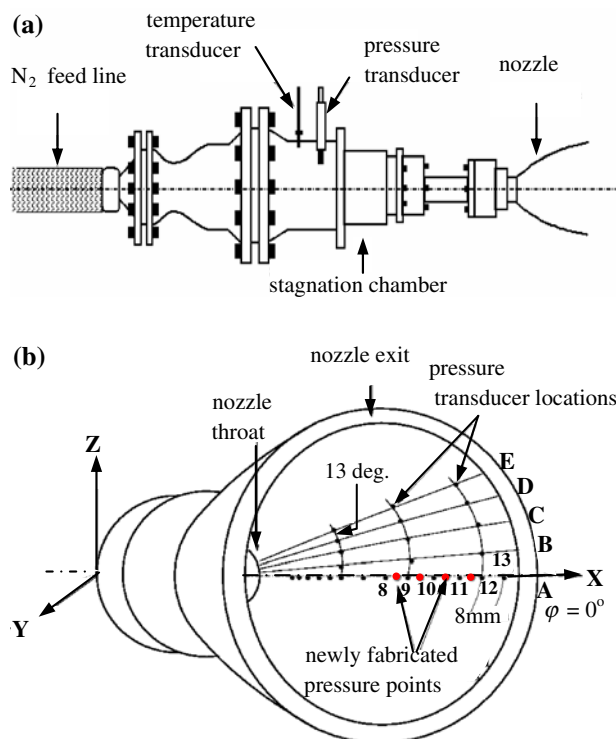


Fig. 2 a Schematic of the nozzle test-facility at DLR P6.2 and b schematic of the pressure sensor locations and the choice of axis

a single axial line in the supersonic section of the nozzle (with a pitch of 8 mm, sampling frequency 25 kHz with low-pass filter cut-off frequency of 8 kHz). In addition to these, 4 more pressure points were fabricated recently, one each midway between the pressure points 8 to 12 in order to capture flow details during RSS at various NPR. Figure 2b shows the choice of axis and the pressure transducer locations for the present tests. A data acquisition system is used which has the capacity of measuring 64 channels at 1 kHz and 16 at 50 kHz or 8 at 100 kHz. Surface flow patterns were visualized using the classic oil pigment mixture (using vacuum pump oil, titanium dioxide and oelic acid) which helped reveal important surface flow information at various nozzle operating conditions. Online recording of visualization tests was done with a camera looking up into the nozzle which was later digitized to extract vital flow information such as subtle movements of the physical separation location especially during ‘pRSS’ condition.

Contrary to usual side load measurement devices, where forces perpendicular to the nozzle axis are determined by measuring the resulting torque with respect to a cardan point, the P6.2 test stand uses, inspired by Dumnov et al. [32], a simple, very thin-walled bending tube, made of a special aluminium-alloy that is mounted upstream the convergent nozzle part (Fig. 3). It resists the high nozzle feeding pressure, but is still sensitive to lateral forces. Pairs of two strain

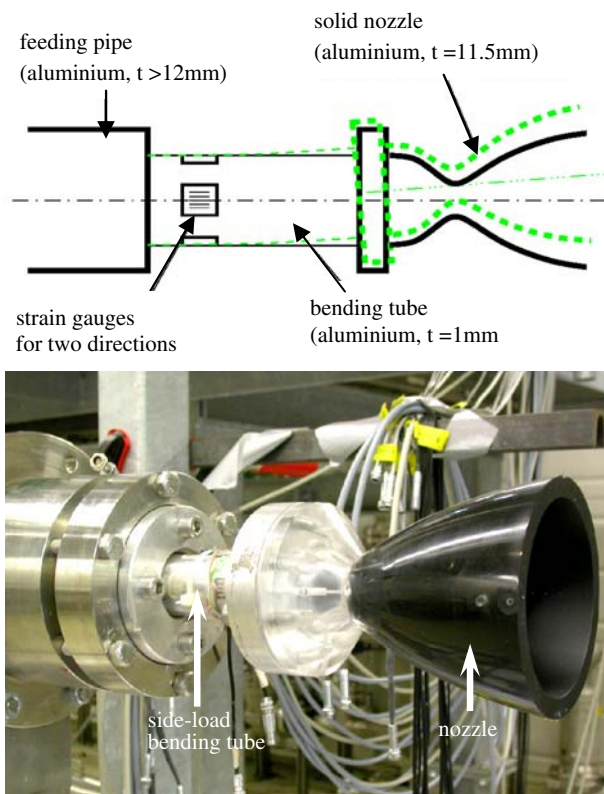


Fig. 3 P6.2 side load measurement device

gauges are applied in each quadrant. Opposite pairs build a full Wheatstone bridge to measure one of the two lateral directions. Due to the wiring only bending strains are measured. All other strains, provoked by the inside pressure, the longitudinal nozzle force and temperature effects, are compensated. The first eigen frequency of the bending tube calibrated under static tests was found to be 73.245 Hz.

3 Results and discussions

3.1 Side-load activity

Flow separation in an overexpanded nozzle is often accompanied by wall pressure fluctuations both in the separation and separated regions. These fluctuating wall pressures act on the nozzle shell resulting in vibrations of the complete nozzle assembly. The main source of lateral-forces/side-loads in rocket engines, initially, was thought of mainly due to asymmetry of separation location along the nozzle circumference. However, ground tests of the J-2S engine [2] revealed flow transitions inside the nozzle as another major source of side-load origin which were later studied extensively at DLR Lampoldshausen [4–6], both experimentally and numerically. Intensive side-loads, originating because of the

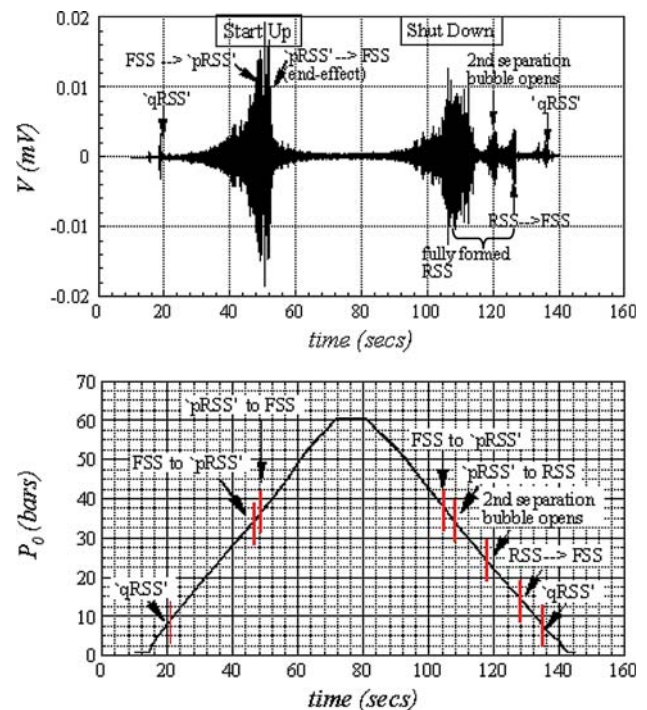


Fig. 4 Strain gauge signal in XY direction from one of the test campaigns showing the appearance of peaks (signifying the existence of lateral forces) during start up and shut down phases

above causes, have also been observed in the developmental stages of main engines such as the J2-S, RD-0120 and Vulcain 1 & 2 [33]. Intense side-load activity has also been revealed in the sub-scale tests [4–6, 29] with the origin of peaks in side-loads being correlated to the prevalent flow transition conditions in the nozzle.

Figure 4a and b shows the time-history of strain-gauge signal in X–Y direction and the corresponding stagnation pressure history, respectively, for one complete test run. The peaks in the strain gauge voltage indicate the various flow/flow-transition conditions experienced during the test run (as shown). For start up phase, for example, three major peaks in signal are observed. The first at NPR \sim 9.75, second for NPR between 35 and 37 while the third between NPR = 38 and 40. Each of the above peaks are known now as a result of quasi-restricted shock separation ('qRSS') [34], FSS \rightarrow 'pRSS' [25] and 'pRSS' \rightarrow FSS [2, 25, 29], respectively. During shut down, however, four main peaks are observed which are mainly attributed to the formation of restricted shock separation (FSS \rightarrow RSS), the formation/opening of a second separation bubble, RSS \rightarrow FSS [30] and qRSS [34].

Figure 5a shows the evolution of maximum *rms* levels at various NPR for both start up ($\delta P_0/\delta t > 0$) and shut down ($\delta P_0/\delta t < 0$) conditions in the separation region. Each of these points correspond to the maximum value of *rms* level (in separation region) obtained from streamwise *rms* distribution of wall pressure signals at each NPR. Earlier Verma

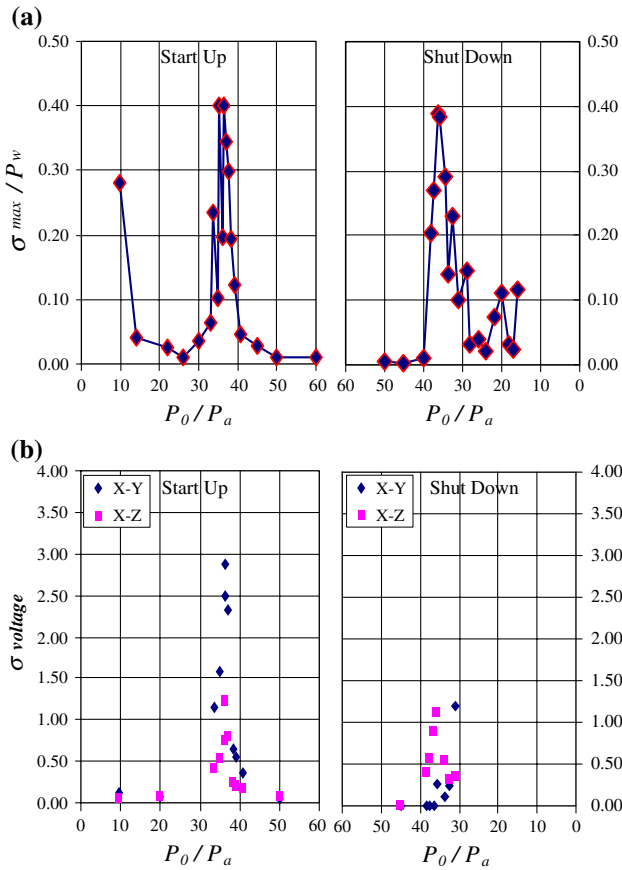


Fig. 5 a Plot of maximum rms level in the intermittent separation region for start up and shut down sequences. b Evolution of rms levels of strain gauge signals; for both cases in (a) and (b), steady upstream stagnations conditions exist at each NPR tested

et al. [25] reported that the unsteadiness preceding the flow-transitions are related to origin of lateral-forces/side-loads in nozzles, which is apparent from Figs. 4a and 5a. Comparing Fig. 5b (which shows evolution of rms levels of strain gauge signals with respect to nozzle pressure ratio) with Fig. 5a shows that the NPR at which peaks appear in both cases coincide (it has to be mentioned here that the results presented in these two plots are not from same test campaigns. So the NPR for which rms levels of wall pressure signal are shown in Fig. 5a, do not appear in Fig. 5b as the bending tube was not used while taking pressure measurements in the former case). It can also be observed from Fig. 5b, that the rms levels of strain gauge signal measured in the two planes (X – Y and X – Z) show significant variation in values as the transition condition is approached, although the overall trend remains the same in both planes. This suggests asymmetric flow conditions prevalent during these NPR. The above results, therefore, indicate that the combined effects of flow unsteadiness (related to separation) preceding each flow-transition and the associated flow asymmetry as the plausible sources of side-load origin in a TOP nozzle.

The characteristics of flow unsteadiness prevalent under various conditions of flow separation modes and flow conditions preceding flow transitions are found to be very interesting and are discussed separately in the following sections.

3.2 Start up sequence

3.2.1 Mean pressure distributions

Figure 6a shows the streamwise mean wall pressure distributions for a range of nozzle pressure ratios (NPR) during the start up sequence. Each of these are obtained by holding the stagnation pressure constant for approximately 8 seconds. These distributions can be classified into various flow regimes depending upon the observed strain-gauge signal peaks discussed and the type of pressure distribution. The first flow condition, namely, the ‘qRSS’ condition cannot be identified from this mean pressure distribution plot since this condition is a transient flow regime (occurs for NPR between 7 and 10). Beyond NPR 10, the flow is seen to stabilize (which can be identified from the gradual downstream movement of incipient separation location with increasing NPR) and the FSS regime predominates up to NPR of approximately 36. The third flow condition arises when, with further increase

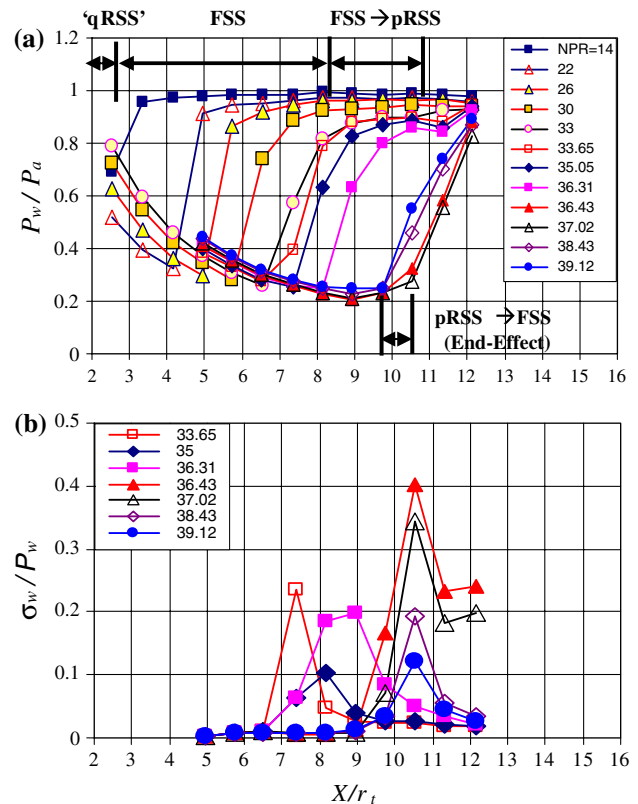
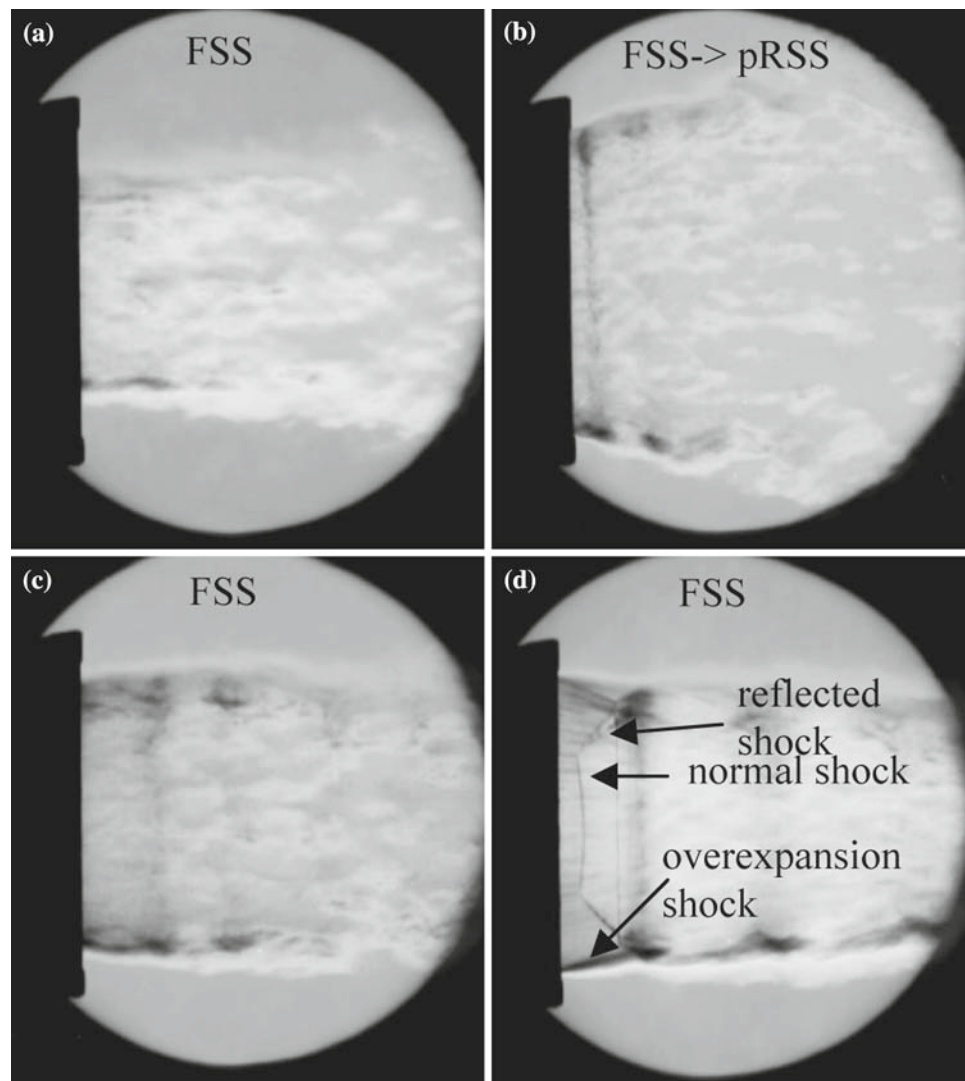


Fig. 6 a Streamwise mean wall pressure and b rms distribution during start up sequence

Fig. 7 Schlieren pictures of the nozzle exhaust flow-field during start up sequence for NPR of **a** 30, **b** 36, **c** 40, **d** 60 (showing the existing shock structure details in a TOP nozzle)



in NPR beyond 36 results in a considerable downstream jump in separation location (four pressure point locations) and marks the flow transition from FSS \rightarrow 'pRSS', shown in Fig. 6a. Between NPR of 36.4 to 37.5, 'pRSS' prevails (identified by lower pressure adaptation (0.83) in the back-flow regime) followed by the end-effect regime ('pRSS' \rightarrow FSS) wherein the incipient separation location jumps upstream (for NPR > 37.5). Once again, a better pressure adaptation of approx. 0.9 is seen for these NPR.

Figure 6b shows the corresponding streamwise *rms* distributions as a function of NPR. It can be seen that each of the above mentioned flow regimes/transitions exhibit some degree of unsteadiness in the separation region (even with steady upstream stagnation conditions) which contributes to the peaks in strain-gauge signal, Fig. 5a. Schlieren pictures show significant changes in the nozzle exhaust flow-field, Fig. 7a–d, when experiencing various separation modes at different NPR. The unsteady flow characteristics for each of these regimes are discussed in the following sections.

3.2.2 Quasi-restricted shock separation (qRSS)

This regime is observed at low NPR both during start up and shut down sequences, as shown in Fig. 4a. Figure 8 shows the time-history of streamwise wall pressure signals and the stagnation pressure history for NPR of 9.75. The wall pressures show fluctuating flow conditions wherein the separation point is seen to move back and forth even though P_0 is held constant. At certain time intervals, the wall pressures at 12th and 13th (close to nozzle exit) pressure transducer locations show P_w values fluctuating above ambient indicating transient flow reattachment. Streamwise mean wall pressure distributions for these time intervals show considerable upstream and downstream movement of the separation point (Fig. 9a). The corresponding *rms* distributions, Fig. 9b, indicate that when the separation point jumps downstream, it exhibits highly unsteady flow conditions with peak in *rms* values going as high as 0.28 in the intermittent separation region. Although 'qRSS' is seen as a highly unsteady

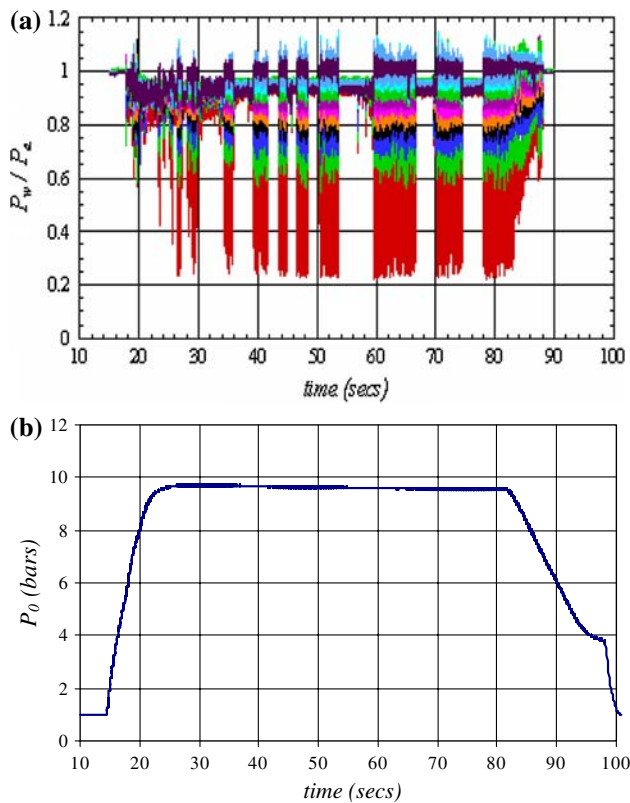


Fig. 8 **a** Time history of streamwise wall pressure signals and **b** the corresponding stagnation pressure; NPR ~ 9.75

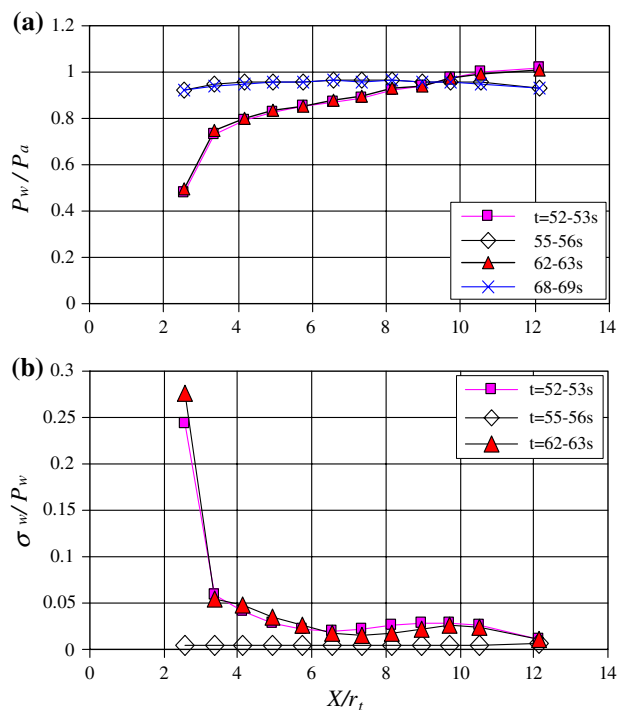


Fig. 9 **a** Streamwise mean wall pressure and **b** rms distribution for 'qRSS' condition; NPR = 9.75

and a transient flow phenomena, both in streamwise and circumferential directions, it does not contribute to relatively significant side-loads, as can be seen in Fig. 4a, primarily due to the low flow momentum associated with it. Further, it may also be pointed out that the observed values of side-load signal are lower due to a smaller lever arm as compared to the situation where side-loads are generated by flow conditions closer to the nozzle exit.

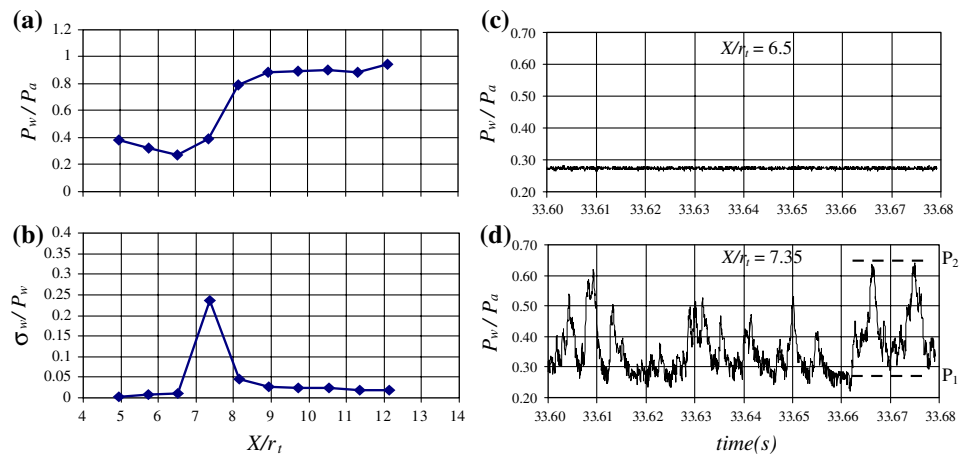
Kwan and Stark [34] identified this phenomenon from their infrared test campaign as quasi restricted shock separation or 'qRSS' meaning that the RSS condition does not occur over a steady state but only as a transient phenomenon. They further showed that the mutual interaction of the shock pattern and the recirculation region behind the cap-shock can cause a short, asymmetric reattachment of the flow on the nozzle wall leading to 'qRSS' condition, that induces lateral forces at low NPR.

3.2.3 Free shock separation (FSS)

Figure 10a and b shows the streamwise mean wall pressure and the corresponding rms distribution for FSS condition at NPR 33.65. The rms distribution displays features typical to SWBLI, i.e., peak in rms value immediately downstream of the incipient separation location indicating high levels of flow fluctuations in the separation region. Figure 10c and d shows the corresponding time-history of wall pressure signals in the separation region. The large-scale streamwise oscillatory motion or 'flapping' of the shock-wave can be easily identified, Fig. 10d. The high-level in wall pressure, P_2 is captured when the "foot" of the shock wave is upstream of the transducer whereas, level P_1 is captured when the shock wave translates downstream of the transducer location. As a result, it can be seen that the sharp rise in rms levels of wall pressure are caused by the intermittent back-and-forth movement of separation/overexpansion shock between levels P_1 and P_2 . The separation region is, therefore, bound by the point of incipient separation (the point at which wall pressure first shows signs of increase from vacuum pressure also known as upstream influence [35]) and the location of physical separation (marked by a distinct line of accumulation of oil pigment). It has been reported earlier [8] that the spatial extent of separation region, i.e., $(X_{sep} - X_{inc})$, tends to increase when the flow undergoes a transition from FSS \rightarrow 'pRSS'.

From Fig. 10d, the pressure ratio between the upstream low-levels and high-levels $\Delta P = P_2/P_1$, can be estimated to about 2.1 on average. Using this value, the point of physical separation can be evaluated which in this case turns out to be approximately at $X/r_t = 7.5$ ($P_w/P_a = 0.476$, which is nothing but the inverse of P_2/P_1 seen from the signal). Careful observation of surface-oil pictures reveal the point of physical separation to approximately coincide with

Fig. 10 **a, b** Streamwise mean wall pressure and rms distribution for FSS condition, $NPR = 33.65$; **c, d** time-history of wall pressure signals in intermittent region of separation



this value. This is an important result that can be used to approximately locate the point of physical separation in nozzle flows with FSS condition. However, the spatial resolution of transducers employed can have significant influence on the detection of intermittent signal in these interactions and hence, affect the true *rms* levels of pressure signals near separation. This was the case in the present study due to the type of kulite model used and the model size.

Aft of separation peak, Fig. 10b, the *rms* level is seen to drop significantly and remains constant up to the nozzle exit. This region corresponds to the back-flow region in nozzles (Fig. 1a), where the ambient air is sucked into the nozzle (adverse pressure gradient) due to the entrainment effect of the separated jet. However, the *rms* level in this region is slightly higher than in its value in the undisturbed boundary-layer. Normally in SWBLI studies on flat plates with fins [36] and compression corners [17, 19], etc. the unsteadiness of the separation shock is attributed to the “breathing” motion of separation bubble formed downstream of separation. However, in FSS condition (with absence of a separation bubble) the only source that can be thought of to trigger shock unsteadiness are fluctuations in the back-flow region. Further with rapid change in mean P_w on either side of this peak, any fluctuations (caused by flow asymmetry along the nozzle circumference) can also cause high levels of fluctuating loads to be generated.

Another way of viewing the separation shock movement is by non-dimensionalizing the instantaneous value of P_{inst} by its mean value, P_w (Fig. 11). This method highlights only those wall pressures fluctuations that change considerably with time above their mean values. It can be seen that the spike, representing the overexpansion compression shock, shows strong variations in its amplitude over time suggesting streamwise movement of the separation shock. No axial movement of this spike was captured since this requires closely spaced wall pressure measurements which

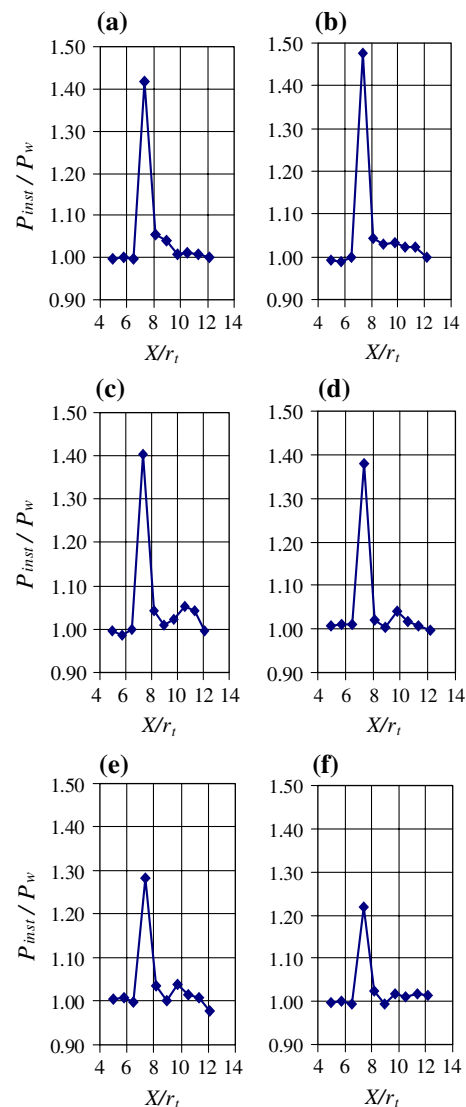


Fig. 11 **a–f** Instantaneous streamwise wall pressure fluctuation P_{inst}/P_w ; each instant separated by time duration of 25 ms

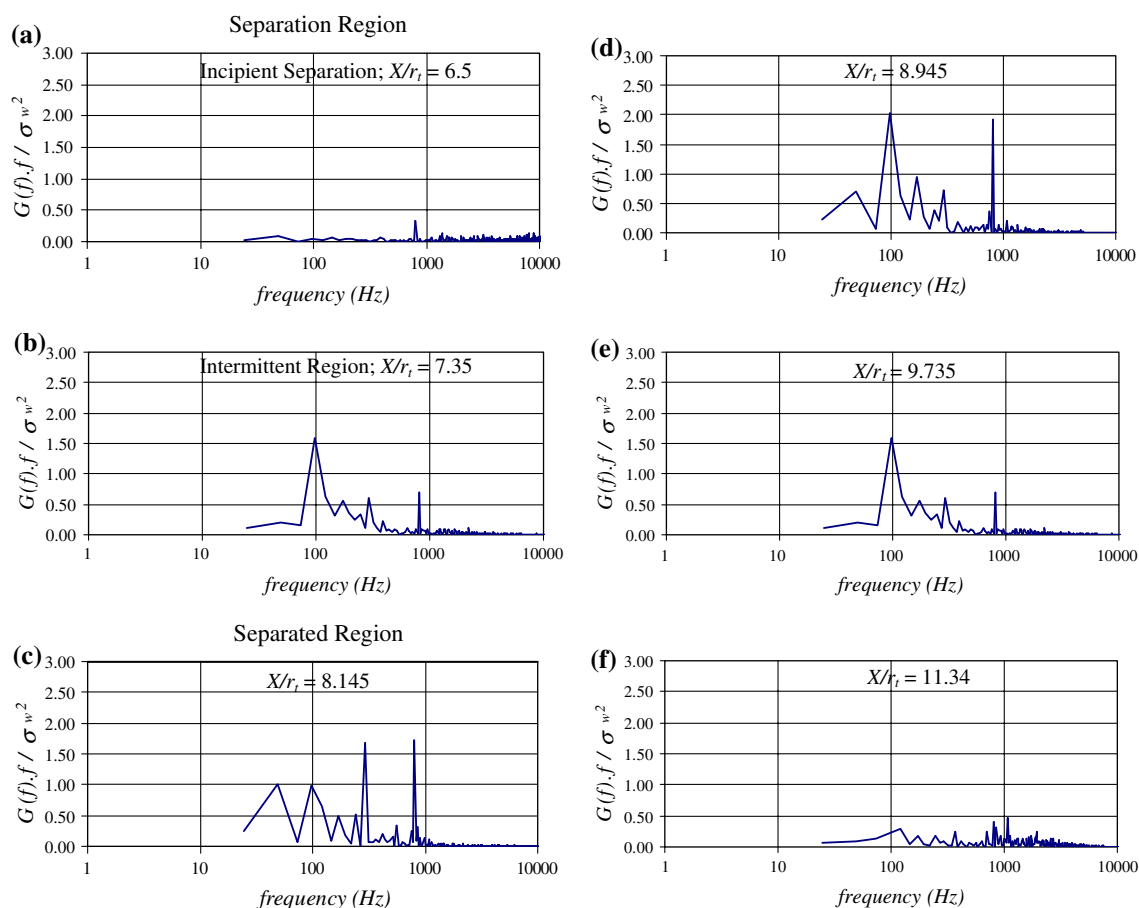


Fig. 12 Evolution of power spectral density along the streamwise direction for $\text{NPR} = 33.65$; FSS flow condition (start up); **a, b** separation region; **c, d** separated region

was not possible with the kulite transducer model used and was also not the prime motive of the study.

Figure 12 shows the longitudinal evolution of power spectra of wall pressure fluctuations in the incipient separation and separated/back-flow regions, respectively. It is known that the power spectral density of the wall pressure signal helps to clearly show the large amplitude, high energy fluctuations, those caused by shock motion, to fall in a fairly narrow low-frequency band. Here $G(f) \cdot f / \sigma_{pw}^2$ is plotted against frequency f on a linear-log scale in order to highlight the dominant frequencies in the signal. It can be seen that the region of incipient separation, Fig. 12a, is essentially dominated by high-frequency fluctuations of very low-amplitude and a low-amplitude low frequency (~ 800 Hz) fluctuation suggesting the upstream extent of intermittent region captured by the pressure signal. In the region of intermittent separation, Fig. 12b, the power spectra shows dominance of low-frequency high-amplitude fluctuations between 100–800 Hz. The separated region, Fig. 12c–f, shows high-amplitude low-frequency contribution with dominant peaks at 300 and 800 Hz. Interestingly, the low-frequency unsteadiness of the moving separation shock is seen to persist downstream

of separated region. Far downstream near the nozzle exit, the power spectra, once again becomes fairly broadband.

The possible physical mechanism responsible for generation of flow unsteadiness during FSS seems to be the back-flow region that is set into pressure pulsations due to the close proximity of turbulent shear-layer, emanating from the separation point, to nozzle wall. This can cause asymmetric pressure distribution in the back-flow region along the nozzle circumference and hence, influence the local position of the separation front through the subsonic re-circulation region. This in turn is a strong function of NPR and the radial size of the recirculation zone defined by $(A_e - A_{\text{sep}})$. High expansion contoured rocket nozzles are generally designed in such a way so as to keep the nozzle exit wall angle $\theta_{w,\text{exit}}$ as small as possible (in order to minimize divergence losses). If we now assume that the nozzle exhaust features remain preserved, then increasing the NPR will go on decreasing the difference in θ_w at X_{sep} and $\theta_{w,\text{exit}}$, i.e., the gap between the nozzle wall and the lower limit of mixing-layer goes on decreasing. This can increase the overall flow unsteadiness downstream of separation which in turn affects the intermittency in the separation region caused by flow

reversal at the location of physical separation. It has been reported [37] that if the value ($A_e - A_{sep}$) is large (as under low NPR conditions), the pressure rise over this zone is negligible. On the other hand, a small radial size shows a strong dependence of P_{pl}/P_a on the contour. The above also suggests that the possibility of initiating flow reattachment (partial or full) increases as the separation location is pushed downstream. Full-scale tests of LE-7A engine [15, 16] have shown transition to RSS condition as soon as an additional skirt is added to the original nozzle. Lawrence and Weynand [38] therefore suggested that the new separation criteria should take into account the influence of contour downstream of separation as it controls the entrainment pressure.

3.2.4 FSS → ‘pRSS’ transition

Verma and Ciezki [30] demonstrated that a downstream jump in separation front (during start up sequence, $\delta P_0/\delta t > 0$) can also lead to a strong side-load condition which is immediately followed by a partially restricted shock separation (‘pRSS’) condition wherein the flow pulsates between FSS and RSS condition as a function of time. It therefore becomes important to study the flow conditions during this transition itself.

Figure 13 shows the time-history of streamwise wall pressure signals from pressure sensors that experience the flow transition for $\phi = 0$ degrees. Careful evaluation of the raw pressure signals in Fig. 13 (by zooming in on the time interval in milliseconds) shows that this transition lasts for about 10 ms and results in a significant downstream jump in separation with wall pressure at the 13th ($X/r_t = 12.135$ and closest to nozzle exit) transducer location fluctuating between its value in the back-flow region and above ambient (Fig. 13). The transducers located at the 8th, 9th and 10th streamwise pressure points for $\phi = 0$ and 180 degrees (circumferentially opposite) also show some interesting features, Fig. 14a and b, respectively. The separation front at circumferentially opposite locations is seen to approach the instant of flow transition at different times indicating considerable flow

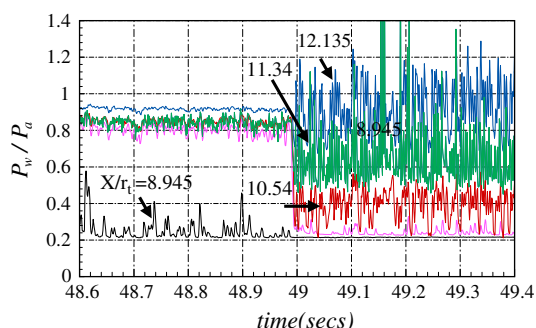


Fig. 13 Wall pressure signals from pressure sensors that experience the FSS → ‘pRSS’ flow transition

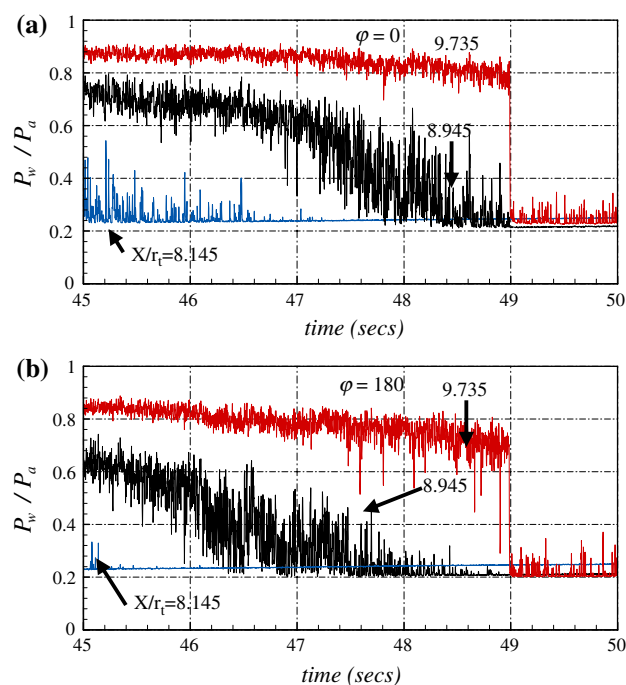


Fig. 14 Time-history of wall pressure signals from pressure sensors placed at $\phi = 0^\circ$ and 180° showing the difference in time of arrival of separation front during the transition process; NPR = 36

asymmetry, Fig. 7(b). This is seen as a significant contribution to the strain-gauge peak during start up with a corresponding high level of *rms* level (Figs. 4a and 5a).

3.2.5 Partially restricted shock separation (pRSS)

Figure 15a and b shows the streamwise mean wall pressure and the corresponding *rms* distribution for NPR = 37.02. Figure 15c–f shows the simultaneously sampled time-histories from wall pressure signals experiencing ‘pRSS’ condition. A striking feature that can be observed from these recorded signals is that the fluctuations of the translating shock in the intermittent separation region are also felt, at the same time instants, by transducers in the separated region especially by those close to the nozzle exit. This suggests flow conditions different from either FSS or RSS (discussed later). Careful visual examination of these pressure signals also reveals that only low-frequency fluctuations behave in this manner. The *rms* distribution, Fig. 15b, also shows high values downstream of the intermittent separation region suggesting the absence of a regular back flow region as seen for FSS condition. The intermittent nature of signals from the 11th, Fig. 15d, and 13th transducer locations, Fig. 15e, poses a question on the physical mechanisms responsible for the high-level fluctuations observed. Visual inspection of the wall pressure signals indicates that P_w at 13th transducer location fluctuates above ambient whenever the separation shock translates back-and-forth in the intermittent region.

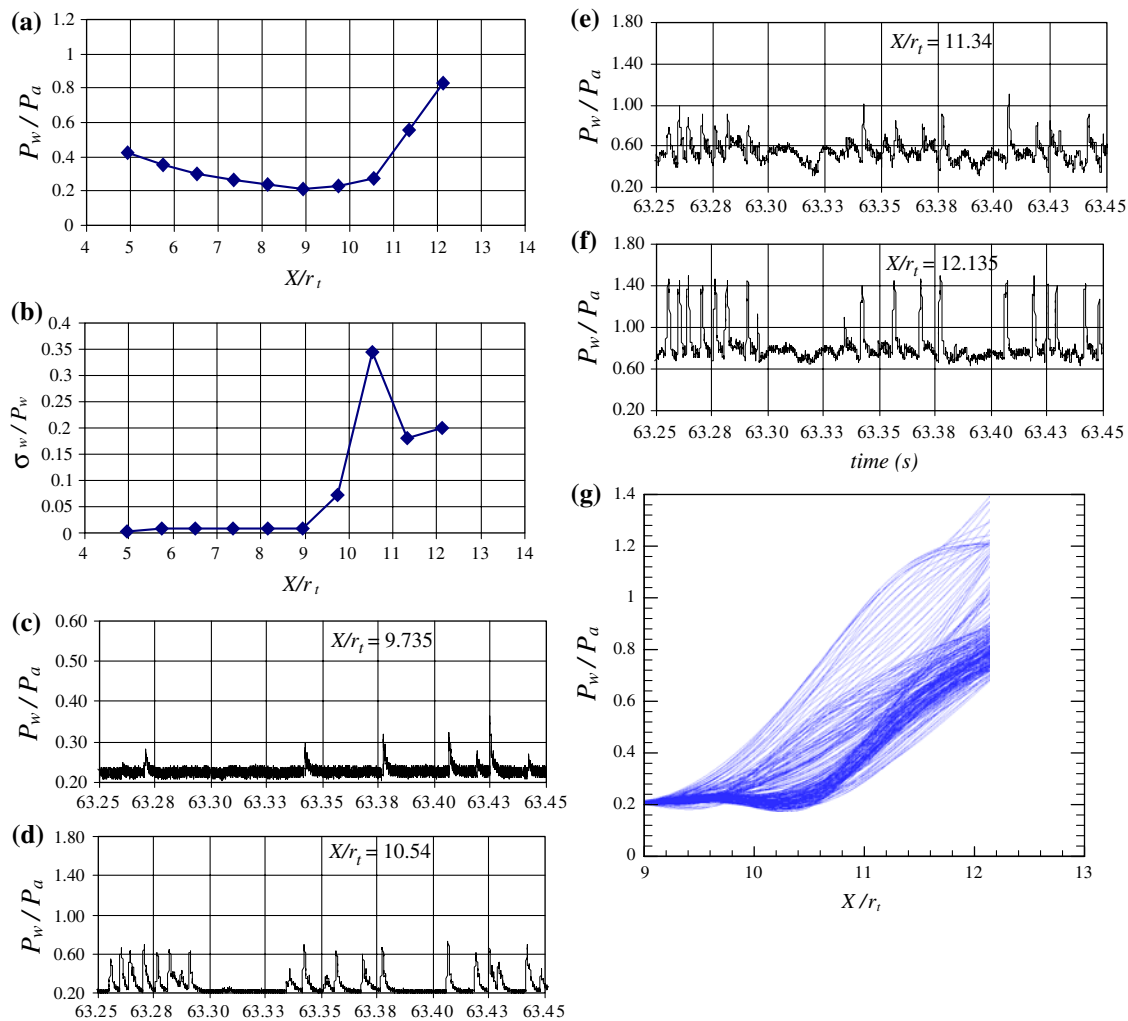


Fig. 15 a, b Streamwise mean wall pressure and rms distribution for pRSS condition, $\text{NPR} = 37.02$; c–f time-history of wall pressure signals in separation and separated regions of the interaction. g Instantaneous wall pressure distribution for pRSS condition, $\text{NPR} = 37.02$; 250 samples

This means that the 13th transducer location experiences random fluctuations of a reattaching flow.

Two types of flow mechanisms can be thought of to generate this type of intermittent pressure signals; firstly, a fully reattached flow with both separation and reattachment shocks translating back-and-forth over the transducers, the fluctuations being initiated by the ‘breathing’ motion of the separation bubble. It has been hypothesized by Garg and Settles [35] that in reattaching flows in SWBLI, the attachment stream surface originates in the freestream flow and lies close to the boundary-layer edge. It therefore, passes close to the foot of the separation shock, forms the upper edge of the separation bubble and then turned back towards the wall surface by the reattaching shock, finally becoming a part of the impinging jet. As a result, it is possible to transmit the intermittent motion of separation shock to the reattachment shock [35]. The second scenario is the random opening and closing of the separation bubble due to close proximity of

the lower limit of the mixing-layer emanating from the separation point to nozzle exit preventing formation of a fully reattached region. The latter case has been identified in nozzle flows [8, 25, 29] and is being discussed here. Figure 15g shows the instantaneous wall pressure distributions with a sampling time interval of 10ms and involving 250 samples. The flow phenomenon indicates more occurrences of FSS condition than RSS. This observation was earlier reported [25] using oil-visualization studies where a prominent separation line could be seen slightly downstream of the 11th pressure point (i.e., $X/r_t \sim 10.84$). However, due to the close proximity, the separated turbulent shear-layer tends to impinge and reattach to the nozzle wall temporarily. When this happens, the separation point is pushed upstream for that time interval. The pulsating nature of separation bubble perhaps once again pushes the flow downstream and the process continues. Figure 16 shows the high-speed (2 kHz) schlieren pictures of exhaust flow-field during ‘pRSS’.

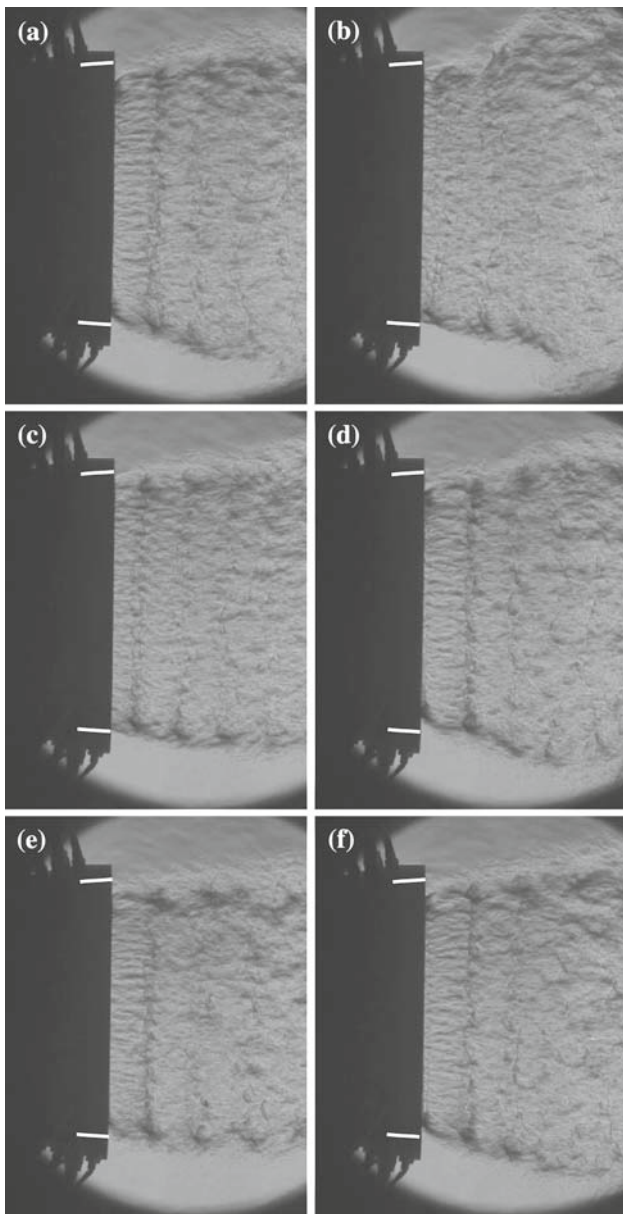


Fig. 16 High-speed schlieren pictures (2 kHz) for ‘pRSS’ condition, $NPR = 37.02$; pictures are arranged from *left to right* in the order of events captured

Another very interesting observation earlier reported by Verma and Haidn [39] is that the flow during shut down does not initiate RSS condition at all if the NPR during start up does not cross a value of 37. What this suggests is that for $NPR > 37$ or so, the relative positions of normal and separation shocks either tend to cross-over or come close to each other. And once this happens, the process is irreversible during shut down suggesting a “hysteresis”. It has been shown earlier [5] that the axial position of normal shock moves faster downstream than separation point at lower NPR while at intermediate NPR, the separation point moves faster towards the nozzle exit. *This non-uniform movement of the*

relative positions of normal and separation shock [5,25] in combination with the changing radial size of the recirculation zone ($A_e - A_{sep}$) can initiate flow unsteadiness in the back-flow region. Such a transition processes could initially be unstable thereby causing random switching of modes between FSS and RSS. However, the flow phenomenon during ‘pRSS’ is not periodic but random in nature. The random nature of intermittent pressure signals can be identified from Fig. 15c–f. The power spectra of pressure fluctuations, Fig. 17, lend some support to this view and shows low

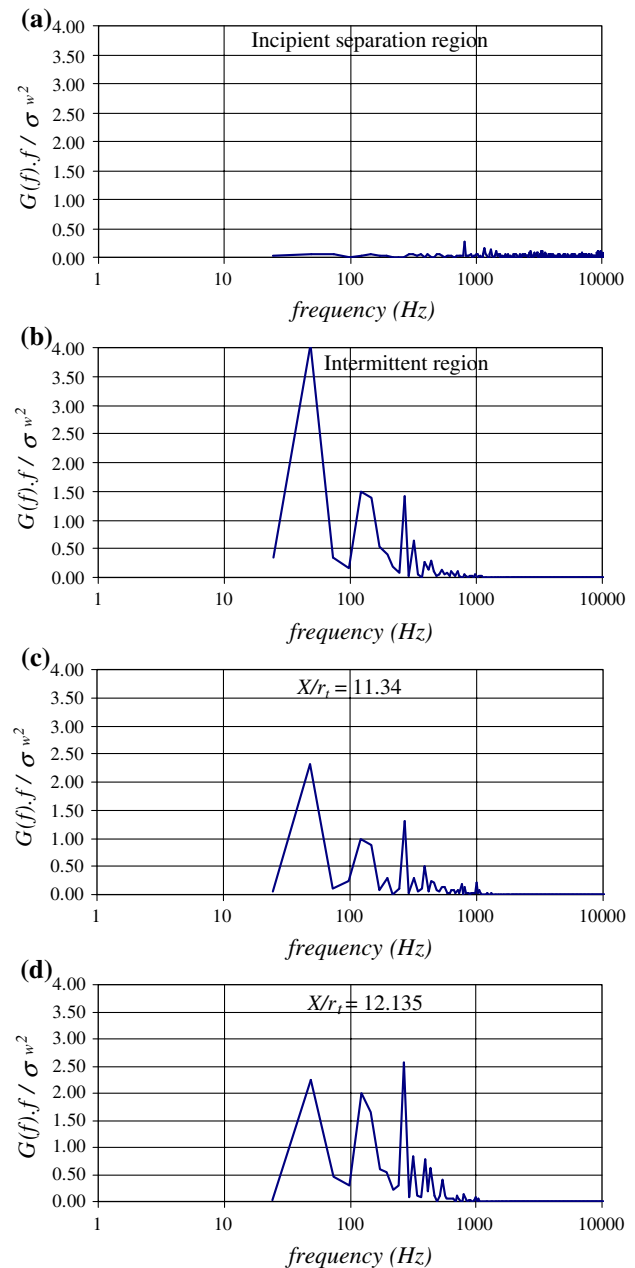


Fig. 17 Evolution of power spectral density along the stream-wise direction for $NPR = 37.02$; ‘pFSS’ flow condition (Start Up); **a, b** separation region and **c, d** separated region

frequency high amplitude random phenomena with absence of any discrete frequency peak.

3.2.6 End-effect flow conditions

Another flow regime that needs scrutiny is the end-effect regime first qualified by Nave and Coffey [2]. This is a flow condition wherein the point of reattachment (in our case ‘partial reattachment’) reaches the nozzle lip and the recirculation bubble completely opens to ambience. Due to the adverse pressure gradient the ambient air rushes in causing the separation location to jump upstream [8] leading to ‘pRSS’ → FSS transition (seen as a better pressure adaptation to ambient in the back-flow region, Fig. 6a). Ideally this could, once again, trigger impingement of separated shear-layer to the nozzle wall and we would again witness a FSS → ‘pRSS’ transition. But it does not happen this time. This means, despite the all the physical mechanisms discussed in the preceding section that favor ‘pRSS’ condition for $NPR < 37.5$, the flow conditions now do not favor FSS → ‘pRSS’ for $NPR > 38$. This emphasizes the fact that once the normal shock position moves downstream of the separation shock location, the momentum imbalance supports only FSS condition. The resulting shock interaction raises the relative position of separated shear layer from the nozzle wall preventing further possibilities of jet impingement. The flow therefore, begins to stabilize showing reduced levels of *rms* peak (in separation region) as the separation point is pushed downstream with increasing NPR thereafter, Fig. 6b.

3.2.7 Three-dimensionality of separation shock-front

Shock-wave boundary-layer interaction phenomena in two-dimensional flows have always discussed the layered look of the shock-plane which has often raised questions about its interpretation [22]. Figure 18a–c shows a series of schlieren pictures (top to bottom) of the exhaust flow-field from a TOP nozzle at $NPR = 52$ with knife edge parallel to flow. Other than the broad features of shock-structure typical to TOP nozzle exhaust, a striking feature is the presence of longitudinal streaks in the flow that end up at the origin of the ring of expansion fan (outer jet) [25]. Two types of flows can be thought of to create such an impression, one being the presence of Goertler vortices and the other, the layer look of separation shock-front. The possibility of the existence of Goertler vortices in FSS conditions is completely ruled out as these have been observed (from the detailed surface oil-visualization studies of Verma and Haidn [39]) during RSS condition only. Also, Goertler vortices are known to be stationary in nature [40,41] and if present, do not show spatial movements with time. Earlier studies [25] show movement of these longitudinal streaks with time suggesting the possibility of some other flow phenomena.

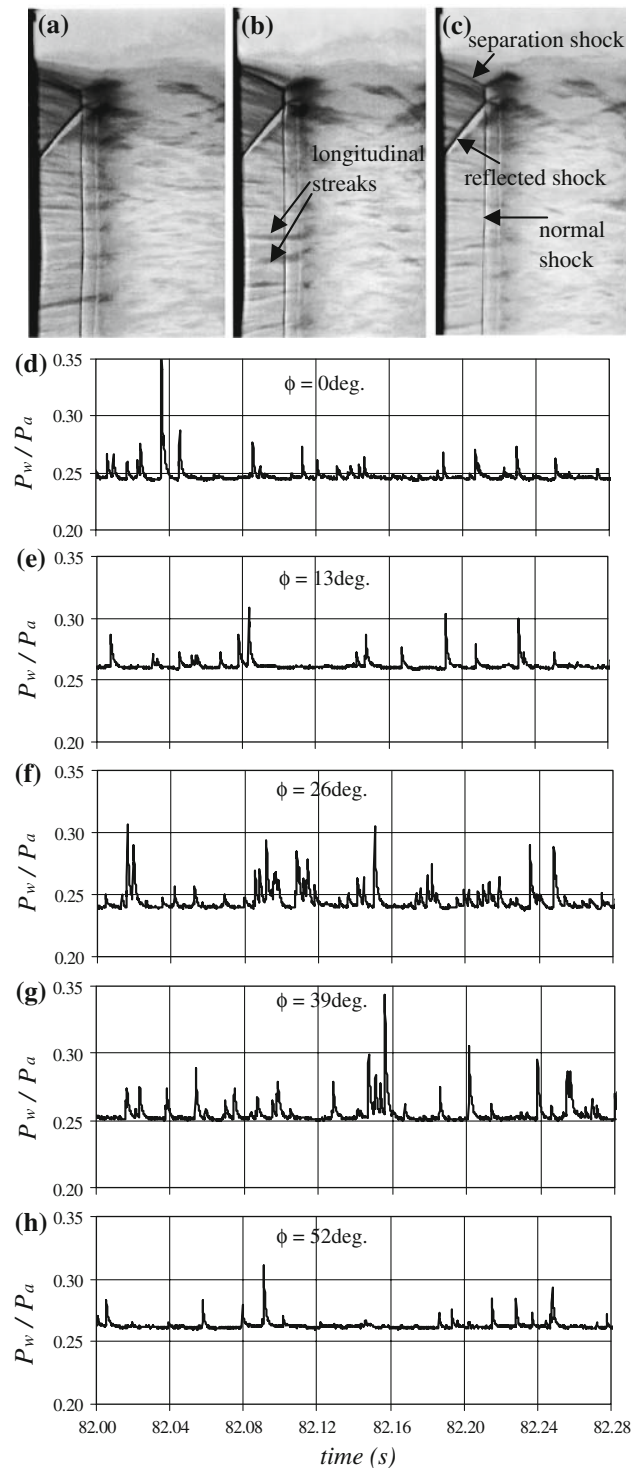


Fig. 18 Schlieren pictures showing movement of longitudinal streaks in the separation shock plane, each frame is separated by a time interval of 1 s; a–e time history of wall pressure signals from circumferentially placed transducers at same streamwise location, $X/r_t = 11.34$; $NPR = 52$

Figure 18d–h shows the time-history of wall pressure signals from circumferentially placed transducer array (5 in number) and measured at only one streamwise location

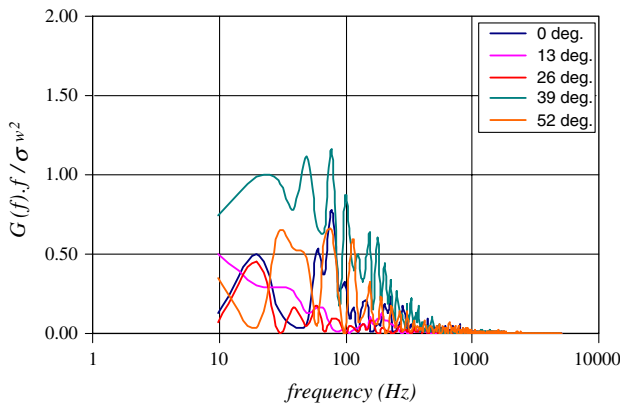


Fig. 19 Power spectral density along the circumferential direction for NPR = 52 capturing the rippling motion of the separation shock plane

($X/r_t = 11.34$). The signal traces clearly show that the shock-front is not two-dimensional but exhibits significant spanwise ripples. This indicates that the circumferential shock-front translates the various transducer locations at different time intervals. The spanwise folding/ripple creates a small region of local density-gradient which is seen as a dark streak in the schlieren picture. Power spectra of the fluctuat-

ing wall pressure signals indicate the nature of these pulsations to be of high-amplitude low-frequency range (Fig. 19). In 2-D flows, the origin of these ripples have been thought of due to the turbulent structures in the incoming tunnel-wall boundary-layer [22,36,41,42]. In addition to this, in nozzle flows, their origin could be perhaps triggered by the fluctuating flow in the back-flow region caused by the aspiration effect of the turbulent structures in the separated jet being convected downstream.

3.3 Shut down process

3.3.1 End effect-regime

It is interesting to look into the end flow effects that are once again experienced when the nozzle pressure ratio is decreased ($\delta P_0/\delta t < 0$) gradually. Here the physical separation location, which starts to move upstream with decreasing NPR suddenly shows a downstream jump in its location [25]. Thereafter, instead of a ‘pRSS’ \rightarrow FSS transition (as seen during start up) a ‘pRSS’ \rightarrow RSS transition occurs.

Figures 20a and b show the streamwise mean wall pressure and the corresponding *rms* distributions, respectively,

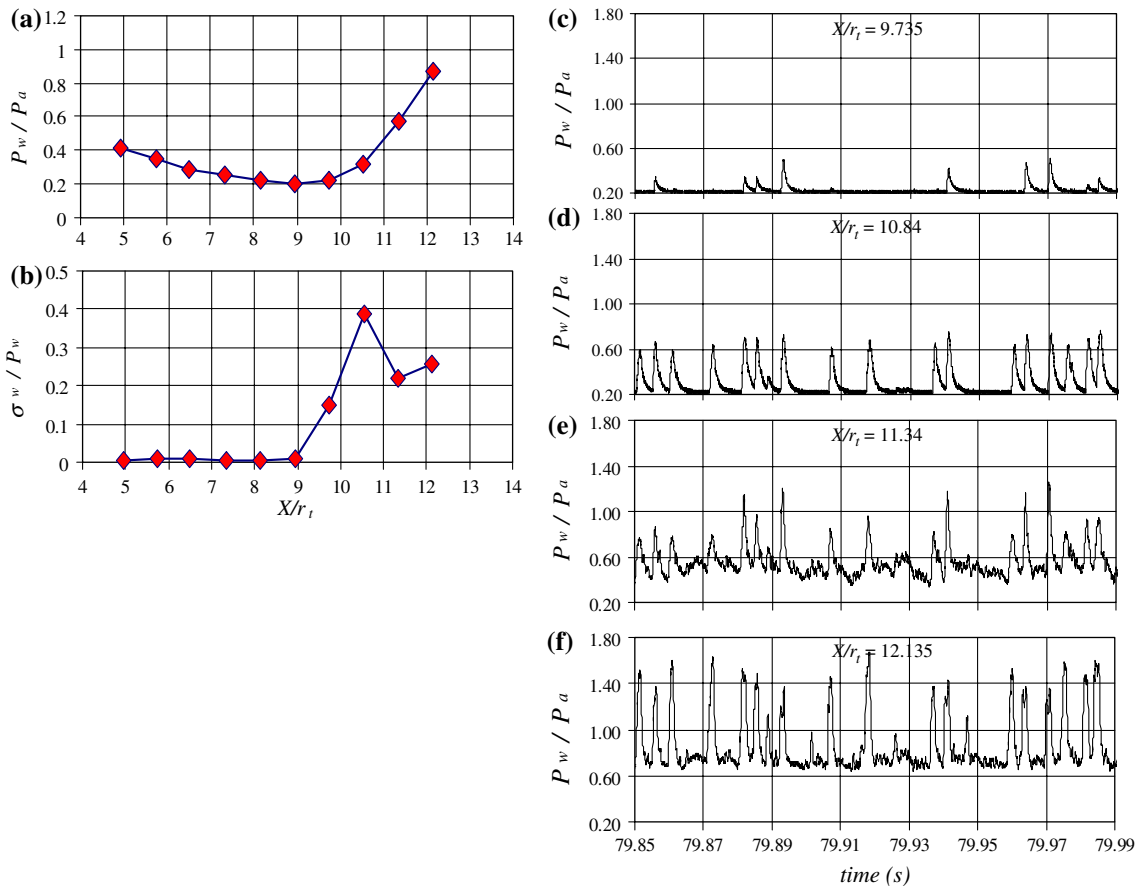


Fig. 20 a, b Streamwise mean wall pressure and rms distribution for pRSS condition, NPR = 36.4; c-f time-history of wall pressure signals in separation and separated regions of the interaction

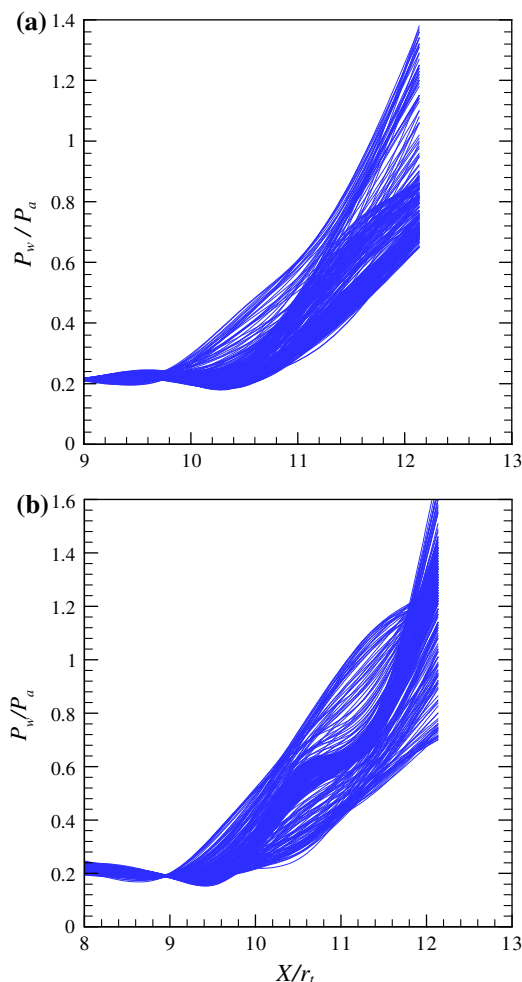


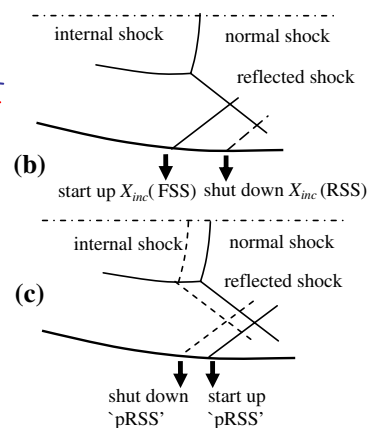
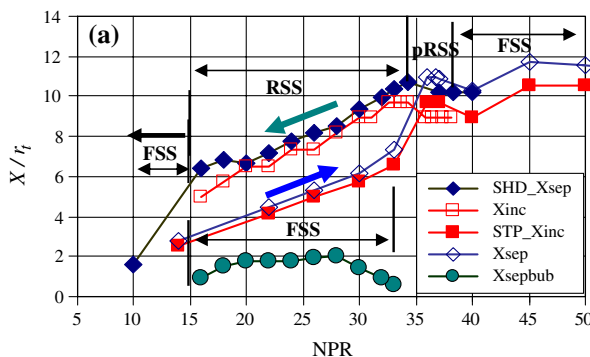
Fig. 21 Instantaneous wall pressure distribution for end-effect regime during shut down (a) NPR = 36.4 and (b) NPR = 34.3; 250 samples

for NPR = 36.4. The magnitude of peak in *rms* pressure level is observed to be slightly larger than the value measured for ‘pRSS’ during start up suggesting similar intermittent conditions. Figure 18c–f show the corresponding simulta-

neously sampled time-histories from wall pressure signals in separation and separated regions. A striking similarity in the overall intermittent nature of wall pressure signals can be seen with those measured for ‘pRSS’ during start up (Fig. 15c–f). However, careful visual examination reveals that the flow intermittency during shut down is not occurring in random batches, Fig. 15d, but seems to be continuously distributed in a random fashion. The spectral characteristics are also very similar to those seen for start up case (and so are not shown). The instantaneous wall pressure distributions (with a sampling time interval of 10 ms and involving 250 samples) show that FSS tends to occur more often than RSS at this NPR (Fig. 21a). On gradually decreasing the NPR further, the instantaneous wall pressure distribution (for NPR = 34.3) begins to show tendency for RSS occurrences more than for FSS (Fig. 21b). The surface oil-visualization movies at this point of time tend to show a downstream jump and thereafter, a prominent formation of physical separation line [25] that is immediately followed by formation of separation bubble in the upstream direction.

To understand the physical mechanisms behind this behavior, the incipient and physical separation locations were plotted for both start up and shut down sequences (Fig. 22). Although the general trend for X_{inc} and X_{sep} with NPR remains the same, a significant shift in their values tells a different story. The ‘pRSS’ regime during shut down is seen to last over a wider range of NPR between 39–35.8 while it is seen to occur only between 36.43–37.5 during start up. So if it is now assumed, that the normal shock moves upstream at the same rate as it moves downstream during start up, then a reduced value of X_{inc} would favor FSS condition (and increase in its value, RSS condition) (Fig. 22b). However a ‘pRSS’ condition is favored instead and that too for a wider range of NPR indicating that the normal shock moves upstream at a much faster rate during shut down (Fig. 22c). Thus a ‘hysteresis’ in the movement of the relative positions of normal and separation shocks occurs. It would be interesting to see if such a ‘hysteresis’ also occurs in hot flows or is it a phenomenon

Fig. 22 a Plot showing the incipient and physical separation locations as a function of NPR for both start up (STP) and shut down (SHD) sequences; b, c schematic illustration of the possible phenomena during shut down



typical to cold-flows. Further studies need to be carried out in this direction.

3.3.2 Fully formed RSS

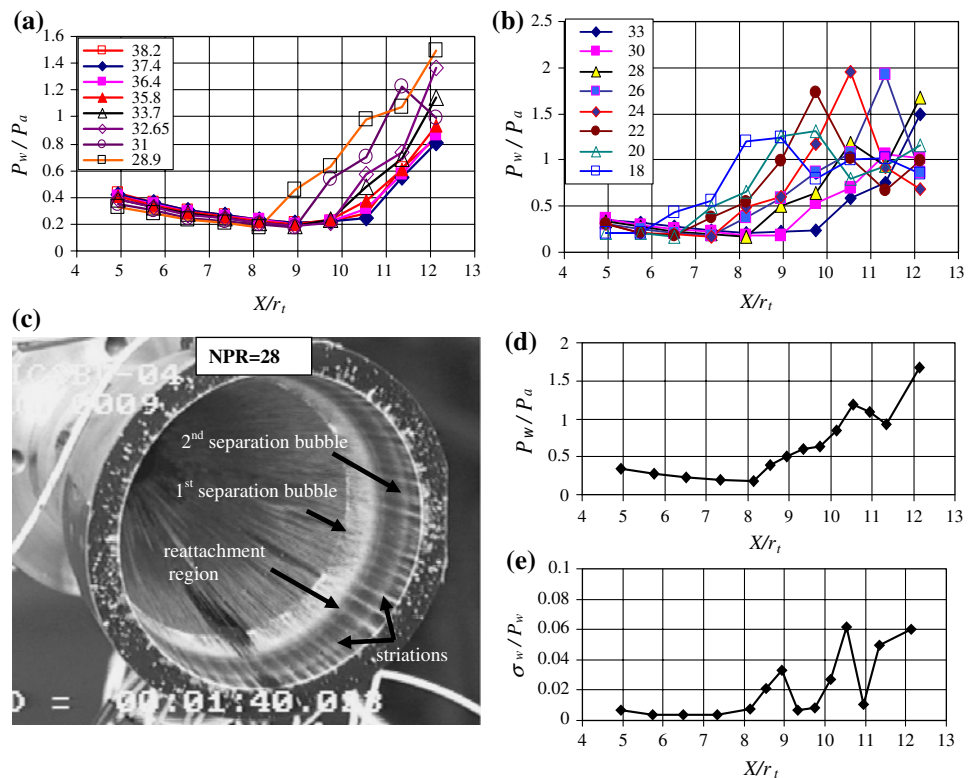
Figure 23a and b shows the streamwise mean wall pressure distribution for a range of nozzle pressure ratios that experience fully formed RSS condition. Comparing each of these conditions with their respective surface oil pictures shows that the mean wall pressure rises gradually in the separation region, tends to level-off somewhat in the fully separated zone, and then starts to rise again in the reattachment region where its value eventually rises above ambient pressure P_a . Downstream of this peak, two types of flow conditions may be observed, firstly, a back-flow region formed as a result of a strong reattachment shock causing the flow to separate (as seen with $P_w < P_a$ near nozzle exit) and secondly, a pressure plateau followed by P_w value once again rising above ambient pressure P_a . The latter case is the one in which a second separation bubble forms downstream of the region of first reattachment finally followed by flow reattachment once again.

Figure 23c–e shows one such case at NPR of 28 at which the second separation bubble forms for the first time during shut down. Downstream of the point of incipient separation, Fig. 23d, a pressure plateau is observed indicating a separation bubble ($P_w < P_a$) after which the wall pressure rises above ambient indicating a reattachment region ($P_w > P_a$).

Downstream of reattachment, P_w falls below P_a and then again rises above P_a . Comparing this plot with the corresponding oil-visualization picture taken during the test run, see Fig. 23c, indicates that the flow forms two separation bubbles and reattaches twice. The spatial extent, however, of each of the separation bubbles is dictated by the complex system of shocks in the annular jet. The surface-oil picture clearly shows that the second separation bubble is very small relative to the first one. Stark et al. [43] (using IR thermometry) and Nguyen [29] (oil studies) also reported observing the presence of a second separation bubble during RSS. Infrared thermometry studies by Gross et al. [44] and Stark et al. [43] during RSS condition report the nozzle wall to be exposed to rather high heat flux in the vicinity of the reattachment line. Also interesting to observe are striation patterns all along the nozzle circumference which indicate the presence of Goertler vortices [39,43,44] formed due to the concavity of reattaching boundary-layer.

Figure 23e shows the corresponding streamwise *rms* distribution for the case discussed above. As expected, peaks in *rms* value are observed in both separation and reattachment regions. The position of first reattachment line is seen to approximately coincide with location of first peak in mean pressure distribution. Since large mean pressure gradients exist in the vicinity of reattachment line, the random fluctuations in the instantaneous position of reattachment shock will cause high fluctuating pressure levels to be generated. The *rms* value then drops in the vicinity of the second

Fig. 23 Streamwise mean wall pressure distribution for a range of NPR during shut down (a) near effect regime NPR; (b) fully formed RSS NPR; (c) surface oil picture for RSS condition at NPR = 28; (d) streamwise mean wall pressure and (e) *rms* distribution for NPR = 28



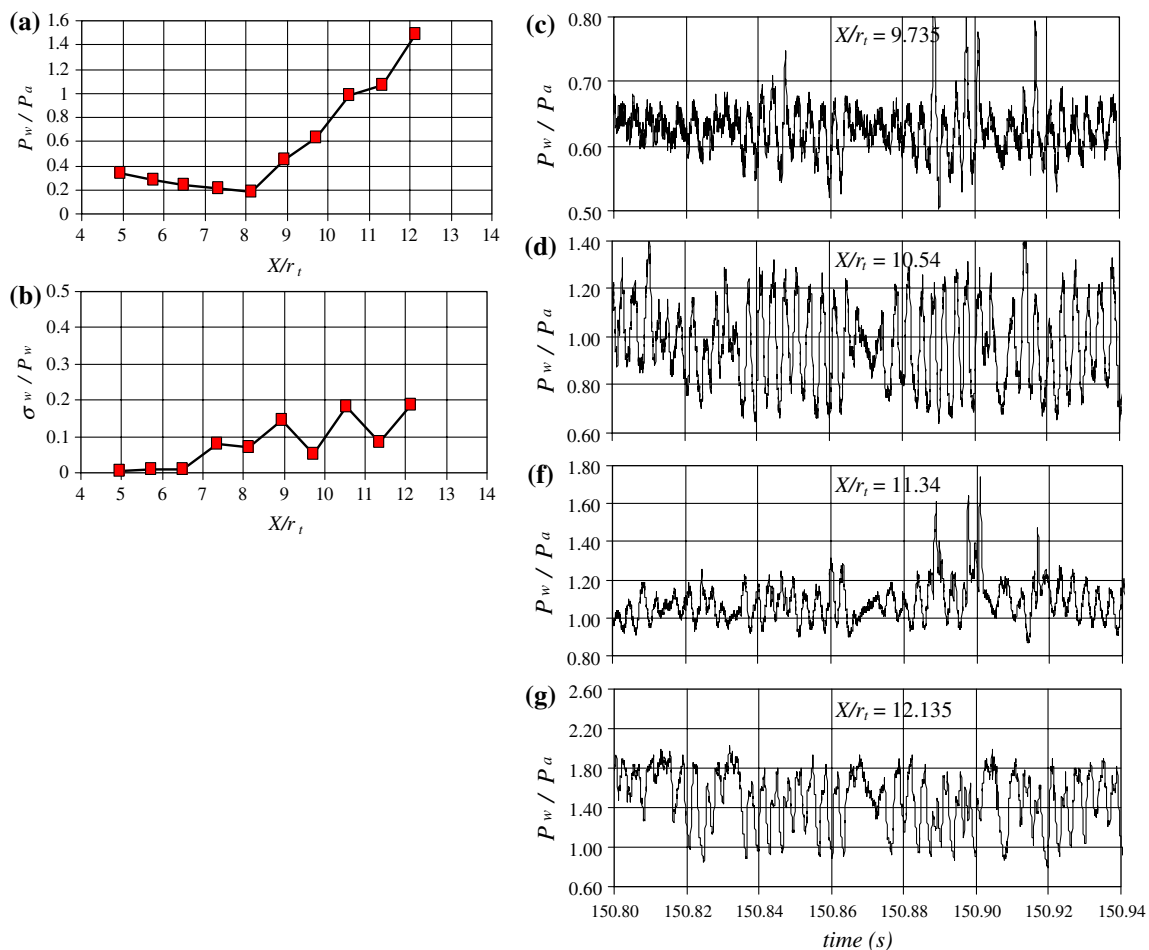


Fig. 24 a, b Streamwise mean wall pressure and *rms* distribution for RSS condition, NPR = 28.9; c–f time-history of wall pressure signals in separation and separated regions of the interaction

separation bubble before finally rising as the point of second reattachment is approached.

In order to understand the flow characteristics of fully reattached flows, a case for $\text{NPR} = 28.9$ is studied in detail (Fig. 24a, b). Figure 24c–f shows the time-history of wall pressure signals from transducer placed at 10th, 11th, 12th and 13th, as shown. A striking feature of wall pressure signals is that the nature of pressure fluctuations in the separation region do not exhibit any of the characteristics of intermittent separation. Rather the characteristics suggest a flow phenomenon of oscillatory/periodic nature. Another interesting flow feature observed from the time traces of 11th, 12th and 13th transducer locations is that the pressure signals from 11th and 13th locations change in concert with one another, whereas those at locations 11th and 12th or 12th and 13th follow opposite trends, almost to the extent of mirror imaging. The above trends are, however, observed for relatively low-frequency fluctuations while the high-frequency changes in pressure signal may not necessarily follow the same. Streamwise evolution of power

spectra shows only a single prominent high-amplitude low-frequency peak (~ 300 Hz) of pressure fluctuations in the interaction region indicating that the unsteadiness in RSS condition is a periodic phenomena rather than a random one (Fig. 25). This observation is unique to flow reattachment region. Such flow characteristics of pressure signals give an important insight of the prevalent flow conditions during fully formed RSS in nozzle flows.

4 Conclusions

Fluctuating wall pressure measurements have been made for various separation modes experienced by the flow during start up and shut down sequences in an overexpanded TOP nozzle. These include ‘qRSS’, FSS, ‘pRSS’ and fully formed RSS apart from flow transition between them. Measurements were made across the entire interaction region (streamwise as well as in circumferential direction) which helped provide *rms* distributions of wall pressure fluctuation and their

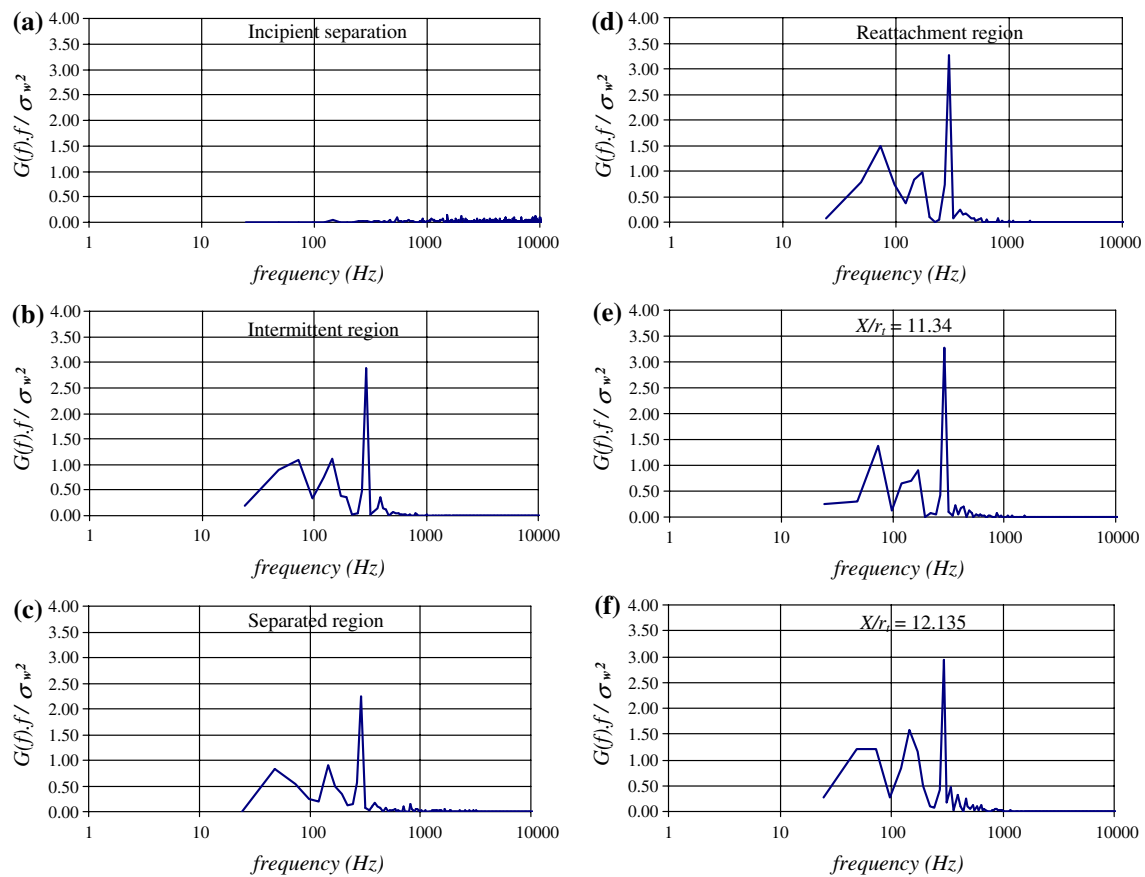


Fig. 25 Evolution of power spectral density along the streamwise direction for $\text{NPR}=28.9$; RSS flow condition (Shut down); **a, b** separation region and **c–f** separated region

corresponding spectral content. The possible physical mechanisms responsible for the origin of overall flow unsteadiness in each of these modes and their contribution towards generation of side-loads are discussed.

On the basis of their observed characteristic features, the shock unsteadiness in nozzle flows can be broadly classified into two types, namely the regular intermittent bi-modal wall pressure signal near separation which is of random nature and the periodic back-and-forth motion of separation shock which causes the entire interaction region to oscillate as a single unit and at a discrete frequency. The former feature of wall pressure signals is observed for ‘qRSS’, ‘pRSS’ and FSS conditions while the latter is unique to RSS condition. In FSS condition, the separation shock is also seen to be highly three-dimensional showing spanwise ripples. Whether random or periodic, the observed fluctuations are of high amplitude and lie in the low frequency range (<1 kHz) of the power spectra. The random and unsteady nature of pressure fluctuations in the separation region are seen to be responsible for the generation of peaks in strain-gauge signal. The unsteadiness preceding transition between various separation modes is not the only source of their origin. Other sources such as random

fluctuation between FSS and RSS, as observed during ‘pRSS’ and unsteadiness of separation front in combination with any flow asymmetry along the nozzle circumference, *even during steady nozzle operation*, also contribute to increases in side-load/strain-gauge condition.

The physical mechanisms responsible for the generation of flow unsteadiness in FSS condition seems to be *the back-flow region that is set into pressure pulsations due to the close proximity of turbulent shear-layer, emanating from the separation point, to nozzle wall. This in turn affects the intermittency in the separation region caused by flow reversal at the location of physical separation and is a strong function of the radial size of the re-circulation zone ($A_e - A_{\text{sep}}$)*. The strongest contribution to the side-load signal during start up is seen when this factor decreases as the separation location is pushed downstream with increasing NPR. In combination to the above, the non-uniform movement of the relative locations of normal and overexpansion shocks also increase flow unsteadiness in the back-flow region as ultimately it is the momentum imbalance of the flow passing through these shocks that dictates the flow condition downstream of separation. RSS condition experiences a periodic ‘breathing’/

‘trembling’ or expansion-contraction motion of the separation bubble that generates an overall unsteady interaction with a discrete peak frequency. A ‘hysteresis’ in the position of normal and separation shock during start up and shut down favors RSS condition during shut down. Further, formation/opening of the second separation bubble also adds to overall increase in flow unsteadiness.

Acknowledgments The results reported in this paper are from the work carried out by the author during his tenure as a research scientist in the Nozzle flow Group at Space Propulsion Institute, DLR Lampoldshausen, Germany between May 2001 to December 2003 and as a Humboldt fellow in 2007. The author would like to thank Ralf Stark, Bernd Wagner and Christian Boehm for their help during the entire course of the test campaign.

References

- Rao, G.V.R.: Exhaust Nozzle Contour of Optimum Thrust. *Jet Propuls.* **28**(6), (1958)
- Foster, C., Summerfield, M., Swan, W.: Flow separation in over-expanded supersonic exhaust nozzles. *Jet Propuls.* **24**(9), 319–321 (1954)
- Nave, L.H., Coffey, G.A.: Sea level side-loads in high area-ratio rocket engines. *AIAA Paper* 73-1284
- Frey, M., Stark, R., Ciezki, H.K., Quessard, F., Kwan, W.: Subscale nozzle testing at the P6.2 test stand. *AIAA* 2000-3777
- Frey, M., Hagemann, G.: Flow separation and side-loads in rocket nozzles. *AIAA* 99-2815
- Frey, M., Hagemann, G.: Restricted shock separation in rocket nozzles. *J. Propuls. Power* **16**(3), 478–484 (2000). doi:[10.2514/2.5593](https://doi.org/10.2514/2.5593)
- Oestlund, J., Damgaard, T., Frey, M.: Side-load phenomena in highly overexpanded rocket nozzles. *J. Propuls. Power* **20**(4), 695–704 (2004). doi:[10.2514/1.3059](https://doi.org/10.2514/1.3059)
- Verma, S.B., Stark, R., Haidn, O.: Relation between shock unsteadiness and the origin of side-loads in a thrust optimized parabolic rocket nozzle. *Aerosp. Sci. Technol. J.* **10**(6) (2006)
- Terhardt, M., Hagemann, G., Frey, M.: Flow separation and side-load behavior in the vulcan engine. *AIAA* 99-2762
- Hagemann, G., Frey, M., Koeschel, W.: Appearance of restricted shock separation in rocket nozzles. *J. Propuls. Power* **18**(3), 577–584 (2002). doi:[10.2514/2.5971](https://doi.org/10.2514/2.5971)
- Onofri, M., Nasuti, F.: The physical origins of side-loads in rocket nozzles. *AIAA* 99-2587
- Reijasse, Ph., Morzenski, L., Naudin, P., Geneau, F.: Fluctuating side-load measurements in overexpanded sub-scale rocket nozzles. *AIAA* 2001-3557
- Morinigo, J.A., Salva, J.J.: Numerical investigation of the separation Modes, transition and hysteresis in the sub-scale J2S rocket engine nozzle. In: 4th International Conference on Launcher Technology, 3–6 December 2002, Liege, Belgium
- Alziary de Roquefort, T.: Unsteadiness and side-loads in overexpanded supersonic nozzles. In: 4th European Symposium of Aerothermodynamics for Space Vehicles, ESA SP-487 (2002)
- Watanabe, Y., Sakazume, N., Tsuboi, M.: LE-7A Engine nozzle problems during the transient operations. *AIAA* 2002-3841
- Watanabe, Y., Sakazume, N., Tsuboi, M.: LE-7A engine separation phenomenon differences of the two nozzle configurations. *AIAA* 2003-4763
- Settles, G.S., Fitzpatrick, T.J., Bogdonoff, S.M.: Detailed study of attached and separated compression corner flowfields in high Reynolds number supersonic flow. *AIAA J.* **17**, 579–585 (1979). doi:[10.2514/3.61180](https://doi.org/10.2514/3.61180)
- Verma, S.B.: Experimental study of flow unsteadiness in a mach 9 compression ramp interaction using a laser schlieren system. *Meas. Sci. Technol. J.* **14**, 989–997 (2003)
- Dolling, D.S., Murphy, M.T.: Unsteadiness of the separation shock wave structure in a supersonic compression ramp flowfield. *AIAA J.* **21**(12), 1628–1634 (1983). doi:[10.2514/3.60163](https://doi.org/10.2514/3.60163)
- Kistler, A.L.: Fluctuating wall pressure under a separated supersonic flow. *J. Acoust. Soc. Am.* **36**(3), 543–550 (1964). doi:[10.1121/1.1918998](https://doi.org/10.1121/1.1918998)
- Dolling, D.S., Narlo II, N.C.: Driving mechanism of unsteady separation shock motion in hypersonic interactive flow. AGARD-CP-428, *Aerodynamics of Hypersonic Lifting Vehicles*, 7–1 to 7–12 (1987)
- Muck, K.C., Andreopoulos, J., Dussauge, J.P.: Unsteady nature of shock-wave/turbulent boundary-layer interaction. *AIAA J.* **26**(2), 179–187 (1988). doi:[10.2514/3.9870](https://doi.org/10.2514/3.9870)
- Muck, K.C., Dussauge, J.P., Bogdonoff, S.M.: Structure of the wall pressure fluctuations in a shock-induced separated turbulent flow. *AIAA* 85-0179
- Poggie, J., Smits, A.J., Glezer, A.: The dynamics and control of fluctuating pressure loads in the reattachment. *AIAA Paper* 92-0178
- Verma, S.B., Haidn, O.: Study on restricted shock separation phenomena in rocket nozzles. *AIAA* 2006-1431
- Smits, A.J., Dussauge, J.P.: *Turbulent shear layers in supersonic flow*. AIP Press (1996)
- Maull, D.J.: Hypersonic Flow over Axially Symmetric Spiked Bodies. *J. Fluid Mech.* **8**, 584–592 (1969). doi:[10.1017/S0022112060000815](https://doi.org/10.1017/S0022112060000815)
- Charwat, A.F., Dewey, C.F., Roos, J.N., Hitz, J.A.: Investigation of separated flows. Part II. flow in cavity and heat transfer. *J. Aeronaut. Sci.* **28**(7), 513–527 (1961)
- Nguyen, A.T., Deniau, H., Girard, S., Alizary de Roquefort, T.: Wall pressure fluctuations in an overexpanded rocket nozzle. *AIAA* 2002-4001
- Deck, S., Nguyen, A.T.: Unsteady side-loads in a thrust optimized contour nozzle at hysteresis regime. *AIAA Journal* **42**(9), 1878–1888
- Verma, S.B., Ciezki, H.K.: Unsteady nature of flow separation inside a thrust optimized parabolic nozzle. *AIAA Paper* AIAA-2003-1139
- Reijasse, P., Corbel, B., Soulevant, D.: Unsteadiness and asymmetry of shock induced separation in a planar two-dimensional nozzle: A flow description. *AIAA* 99-3694
- Dumnov, D.: Unsteady side-load acting on the nozzle with developed separation zone. *AIAA* 96-3220
- Kwan, W., Stark, R.: Flow Separation phenomena in subscale rocket nozzles. *AIAA*-2002-4229
- Garg, S., Settles, G.S.: Unsteady pressure loads generated by swept-shock- wave/boundary-layer interactions. *AIAA J.* **34**(6), 1174–1181 (1996). doi:[10.2514/3.13209](https://doi.org/10.2514/3.13209)
- Dolling, D.S., Bogdonoff, S.M.: An experimental investigation of the unsteady behavior of blunt fin induced shock wave turbulent boundary-layer interaction. *AIAA* 81-1287
- Frey, M., Hagemann, G.: Status of flow separation prediction in rocket nozzles. *AIAA Paper* No-98-3619
- Lawerence, R.A., Weynand, E.E.: Factors affecting flow separation in contoured supersonic nozzles. *AIAA J.* **6**(6), 1159–1160 (1968). doi:[10.2514/3.4693](https://doi.org/10.2514/3.4693)
- Verma, S.B., Haidn, O.: Goertler vortex formation during the shut down sequence inside a thrust optimized parabolic (TOP) rocket nozzle. *AIAA* 2005-518
- Ginoux, J.J.: Streamwise vortices in laminar flow. *AGARDograph* **97**(Part I) (1965)

41. Tani, I.: Production of longitudinal vortices in the boundary layer along a concave wall. *J. Geophys. Res.* **67**, 3075–3080 (1962). doi:[10.1029/JZ067i008p03075](https://doi.org/10.1029/JZ067i008p03075)
42. Andreopoulos, J., Muck, K.C.: Some new aspects of the shock wave boundary-layer interaction in compression ramp flows. *J. Fluid Mech.* **180**, 405–428 (1987). doi:[10.1017/S0022112087001873](https://doi.org/10.1017/S0022112087001873)
43. Stark, R., Kwan, W., Quessard, F., Hagemann, G., Terhardt, M.: Rocket Nozzle Cold-Gas Test Campaigns for Plume Investigations. In: 4th European Symposium on Aerothermodynamics for Space Vehicles, Capua, Italy, October 15–18 (2001)
44. Gross, A., Haidn, O., Stark, R., Zeiss, W., Weber, C., Weiland, C.: Experimental and numerical investigation of heat loads in separated nozzle flow. AIAA 2001-3682